Type-2 Fuzzy Logic Controllers Made Even Simpler: From Design to Deployment for UAVs

Andriy Sarabakha[1,2], *Student Member, IEEE*, Changhong Fu[1,2], *Member, IEEE*,
Erdal Kayacan[1], *Senior Member, IEEE*, and Tufan Kumbasar[3], *Member, IEEE*

Abstract—This paper aims to provide a clear explanation of the role of the footprint of uncertainty (FOU) parameters on the control signal generation and, thus, to increase the interpretability of specially structured interval type-2 (IT2) fuzzy logic controllers, namely single input IT2 fuzzy PID (SI-IT2-FPID) controller. In this context, we extend the analysis performed for SI-IT2-FPID controllers by providing the effect of the FOU parameters on control surface generation. We show that, by only adjusting a single parameter, which shapes the FOU, it is possible to generate commonly employed control surfaces without a requirement of an optimisation assistance. In order to validate our theoretical analysis, we present comparative real world quadcopter flight tests. The real-time experimental results show that the SI-IT2-FPID controller can achieve better control performance in presence of uncertainties and strong wind conditions when compared to its type-1 and conventional counterparts. We believe that the results of this study will open the doors to a wider use of SI-IT2-FPID controllers in real world control applications as the proposed structure is easy to design and feasible to deploy especially in real-time control systems.

Index Terms—Interval type-2 fuzzy logic control, design and deployment, unmanned aerial vehicle, 3D trajectory tracking.

I. INTRODUCTION

UNMANNED aerial vehicles (UAVs) can provide a cheap solution to dull, dirty and dangerous missions, such as aerial inspection [1], territory patrolling [2], midair traffic managment, and cargo transportation [3]. The classical model-based approaches, e.g., PID [4], linear quadratic regulator [5] and model predictive control [6], still seem to be the most widely adopted methods for UAV applications. When the model of the UAV is precise and there are no internal or external uncertainties in the system, these controllers generally provide the optimal performance. However, there are inevitable uncertainties in UAV applications, e.g., lack of modelling, aerodynamic disturbances, changes in the environment, noise on the sensors and actuators. In the presence of the aforementioned uncertainties, which are not supposed to exist in the system throughout a model-based controller design, a model-free controller may be preferable, e.g., fuzzy logic theory [7],

[1]Andriy Sarabakha, Changhong Fu and Erdal Kayacan are with School of Mechanical and Aerospace Engineering, Nanyang Technological University (NTU), 50 Nanyang Avenue, Singapore, 639798. Email: andriy001@e.ntu.edu.sg, changhongfu@ntu.edu.sg, erdal@ntu.edu.sg.
[2]Andriy Sarabakha and Changhong Fu are with ST Engineering-NTU Corp Laboratory, 50 Nanyang Avenue, Singapore, 639798.
[3]Tufan Kumbasar is with the Control and Automation Engineering Department, Faculty of Electrical and Electronics Engineering, Istanbul Technical University, Istanbul TR-34469, Turkey. Email: kumbasart@itu.edu.tr.

[8]. Fuzzy logic control (FLC) is an alternative solution to the model-based controllers in various types of applications, e.g., motor speed regulation [9], inverted pendulum control [10], spherical rolling robot, agricultural mobile robot, marine vehicle control, and flexible spacecraft control. This is due to several features of fuzzy logic controllers, such as improving the robustness of the control system in the presence of uncertainties and external disturbances. Type-1 FLCs (T1-FLCs) are the most well-known and widely used types of FLCs. On the other hand, researchers have recently put significant attention toward more advanced forms of fuzzy logic, such as interval type-2 fuzzy logic controllers (IT2-FLCs) [11], [12]. The transition from type-1 to type-2 has been inspired by the observation that type-1 fuzzy sets can only deal with a limited level of uncertainty whereas real-world control applications are often confronted with high levels of uncertainty [13], [14].

In this study, we aim to explore the potential of interval type-2 fuzzy PID (IT2-FPID) controllers, in particular, single input IT2-FPID (SI-IT2-FPID) controllers, to solve the 3D trajectory following problem of quadcopter UAVs. Although there are a number of FLC applications for navigating a quadcopter UAV in the literature [15]–[18], most of these are T1-FLCs. Another motivation of this study is to investigate how various footprint of uncertainty (FOU) parameter settings (PSs) affect the control performance of the SI-IT2-FPID. Finally, this paper has compared and contrasted the performance of the conventional PID, type-1 fuzzy PID (T1-FPID) and SI-IT2-FPID controllers in real-time. All aforementioned controllers are implemented in robot operating system (ROS).

IT2 fuzzy logic control has had significant impact on real-time control systems, not only it uses expert knowledge as an input to the controller design, but also because of its exceptional ability to deal with uncertainties in the system due to the additional degree of freedom provided by the FOU in their IT2 fuzzy sets. However, due to its relatively more complex internal structure, there is still a need for an interpretable relationship between antecedent IT2 fuzzy sets of IT2 fuzzy logic controller and its control output, i.e., control surface (CS). Motivated by this challenge, the main aim of this study is to contribute to the interpretability of the SI-IT2-FPID controllers by further extending the analysis in [19] and validating several theoretical claims with a real-time UAV trajectory tracking case study under realistic wind conditions. In summary, the main contributions of this study are:

- the analysis in [19], which is based on the *control curve* generation, has been further extended to the *control surface* generation;

- two control signals (φ_p and φ_d) have been combined and their effect has been studied to show the behaviour of IT2-FLC (aggressive, moderate, smooth);
- SI-IT2-FPID controllers are elaborated in terms of their design simplicity as well as interpretability;
- to validate the theoretical claims, real-time applications of SI-IT2-FPIDs are shown for the trajectory tracking problem of quadcopter UAVs under realistic wind conditions.

This paper is organised as follows: Section II introduces the quadcopter UAV's dynamical model and presents the control scheme. Section III reviews SI-IT2-FPID and analyses its properties. Section IV presents the experimental results in order to validate the theoretical claims. Finally, Section V closes this paper with conclusions and future work.

II. QUADCOPTER DYNAMICS AND CONTROL SCHEME

A. Quadcopter Model

In this paper, Parrot Bebop 2 quadcopter UAV, shown in Fig. 1, will act as an experimental platform. The world fixed reference frame is $\mathcal{W} = \{\vec{x}_W, \vec{y}_W, \vec{z}_W\}$ and the body frame is $\mathcal{B} = \{\vec{x}_B, \vec{y}_B, \vec{z}_B\}$. The quadcopter configuration with its reference frames is illustrated in Fig. 1. The absolute position of a quadcopter $\mathbf{p} = \begin{bmatrix} x & y & z \end{bmatrix}^T$ is given by three Cartesian coordinates of its center of mass in $\mathcal{W}$, and its attitude $\mathbf{o} = \begin{bmatrix} \phi & \theta & \psi \end{bmatrix}^T$ is given by three Euler angles. These three angles are called roll, pitch and yaw, respectively. The time derivative of the position gives the linear velocity $\mathbf{v} = \begin{bmatrix} v_x & v_y & v_z \end{bmatrix}^T$ of the quadcopter expressed in $\mathcal{W}$. Similarly, the time derivative of the attitude $\boldsymbol{\omega} = \begin{bmatrix} \dot{\phi} & \dot{\theta} & \dot{\psi} \end{bmatrix}^T$ gives the angular velocity expressed in $\mathcal{W}$, and $\boldsymbol{\omega}_B = \begin{bmatrix} p & q & r \end{bmatrix}^T$ is the angular velocity in $\mathcal{B}$ [20]. The control of translational and rotational motions of the quadcopter are achieved by changing the thrust f_i, $i = 1, \ldots, 4$, of four rotors in different combinations. The thrust from individual rotors is varied by changing their angular speed ω_i, $i = 1, \ldots, 4$. Then, the vector of control inputs $\mathbf{u}$ is chosen as in [21]:

$$\mathbf{u} = \begin{bmatrix} T & \tau_\phi & \tau_\theta & \tau_\psi \end{bmatrix}^T, \tag{1}$$

where T is the total thrust along $\vec{z}_B$, whereas τ_ϕ, τ_θ and τ_ψ are moments around $\vec{x}_B$, $\vec{y}_B$ and $\vec{z}_B$, respectively. Under these considerations, if $\boldsymbol{\Omega} = \begin{bmatrix} \omega_1 & \omega_2 & \omega_3 & \omega_4 \end{bmatrix}^T$, the relation
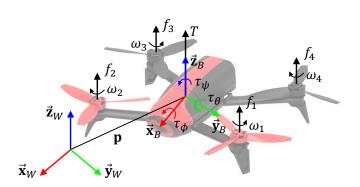
between $\mathbf{u}$ and $\boldsymbol{\Omega}$ becomes linear, static and invertible [22]. Finally, the quadcopter dynamical model is given as in [23]:

$$\begin{cases} \dot{x} = v_x & \dot{v}_x = \frac{1}{m}\left(c_\phi c_\psi s_\theta + s_\phi s_\psi\right)T \\ \dot{y} = v_y & \dot{v}_y = \frac{1}{m}\left(c_\phi s_\psi s_\theta - c_\psi s_\phi\right)T \\ \dot{z} = v_z & \dot{v}_z = \frac{1}{m}c_\phi c_\theta T - g \\ \dot{\phi} = p + s_\phi t_\theta q + c_\phi t_\theta r & \dot{p} = \frac{I_y - I_z}{I_x}qr + \frac{1}{I_x}\tau_\phi \\ \dot{\theta} = c_\phi q - s_\phi r & \dot{q} = \frac{I_z - I_x}{I_y}pr + \frac{1}{I_y}\tau_\theta \\ \dot{\psi} = \frac{s_\phi}{c_\theta}q + \frac{c_\phi}{c_\theta}r & \dot{r} = \frac{I_x - I_y}{I_z}pq + \frac{1}{I_z}\tau_\psi, \end{cases} \tag{2}$$

where m is the quadcopter mass, g is the gravity acceleration ($g = 9.81\text{m/s}^2$), $\mathbf{I} = \text{diag}(I_x, I_y, I_z)$ is the inertia matrix, c_α, s_α and t_α denote $\cos\alpha$, $\sin\alpha$ and $\tan\alpha$, respectively.

Remark 1. *The dynamical equations in (2) are nonlinear, coupled and the system to be controlled is under actuated. Moreover, the UAV must be operated on its unstable equilibrium point.*

B. Control Scheme

The overall structure of the closed-loop control scheme is illustrated in Fig. 2. It consists of three main blocks: position controller, attitude/velocity controller and quadcopter itself. The position controller has three identical and independent sub-controllers for x, y and z axes. If $\mathbf{p}^*$ is the desired position of the UAV and $\mathbf{p}$ is the measured position of the UAV, the position error is $\mathbf{e} = \begin{bmatrix} e_x & e_y & e_z \end{bmatrix}^T = \mathbf{p}^* - \mathbf{p}$. Each sub-controller takes the corresponding position error, as the input, and returns the corresponding control signal, as the output. For the x-axis controller, the input is e_x and the output is the desired pitch θ^*. For the y-axis controller, the input is e_y and the output is the desired roll ϕ^*. For the z-axis controller, the input is e_z and the output is the desired vertical velocity v_z^*. The position controller computes the desired vertical velocity
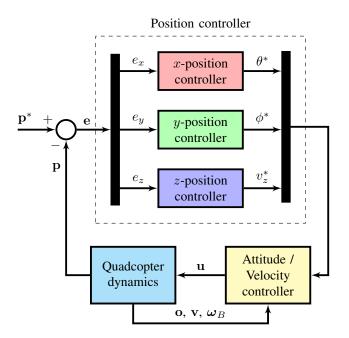

Fig. 1. Parrot Bebop 2 quadcopter UAV with its reference frames.

Fig. 2. Block diagram of the control system for the quadcopter UAV.

v_z^*, desired roll ϕ^* and desired pitch θ^* angles, in order to reach the desired position $\mathbf{p}^*$ from the current position $\mathbf{p}$. The velocity controller computes the desired thrust T in (1) from the desired vertical velocity v_z^* by using the attitude $\mathbf{o}$ and velocity $\mathbf{v}$. For the velocity control, the nonlinear geometric controller on Euclidean group $\mathsf{SE}(3)$ is used. The attitude controller computes the dynamical mapping from the desired roll ϕ^* and pitch θ^* angles to the desired torques $\boldsymbol{\tau} = \begin{bmatrix} \tau_\phi & \tau_\theta & \tau_\psi \end{bmatrix}^T$ in (1). Therefore, the attitude/velocity controller computes the control input $\mathbf{u}$ of the UAV.

III. Interval Type-2 Fuzzy Logic Control

In this section, we will present the general structure of the SI-IT2-FPID controller structure and its design. As it can be observed from Fig. 3, the SI-IT2-FPID structure inherits three IT2 fuzzy mappings (FMs) which shape the proportional, integral and derivative control actions. The input scaling factor k_e is defined such that the input is normalized to the universe of discourse where the antecedent membership functions (MFs) of the SI-IT2-FLCs are defined, i.e., $[-1, 1]$. Thus, after the normalization the error e is converted into σ which is the input to the SI-IT2-FLCs, and their outputs φ_p, φ_i and φ_d are converted into the control signal u as follows:

$$u(\sigma_p, \sigma_i, \sigma_d) = k_p \varphi_p(\sigma_p) + k_i \varphi_i(\sigma_i) + k_d \varphi_d(\sigma_d), \quad (3)$$

where k_p, k_i and k_d are the gains of the baseline PID controller.

The rule structure of each SI-IT2-FLC is as follows:

$$R_i : \text{IF } \sigma \text{ is } \tilde{A}_i, \text{ THEN } \varphi \text{ is } B_i, \quad i = 1, 2, 3, \quad (4)$$

where B_i are the crisp consequents with description on these as $B_1 = -1$, $B_2 = 0$ and $B_3 = 1$. The antecedent MFs are defined with triangular IT2-FSs $\tilde{A}_i$, as represented in Fig. 4. The IT2-FSs are described with an upper MF (UMF) $\overline{\mu}_{\tilde{A}_i}$ and lower MFs $\underline{\mu}_{\tilde{A}_i}$ that provide an extra degree of freedom named as FOU [24]. As shown in Fig. 4, m_i, $i = 1, 2, 3$, represent the height of the lower MFs and they are the parameters which create the FOUs of the IT2-FSs.

In this paper, symmetrical MFs are employed to simplify the design complexity. In this context, we define m_i as follows:

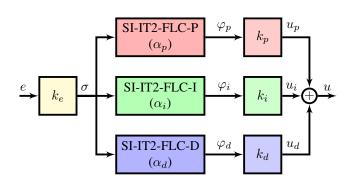$$\begin{cases} m_1 = m_3 = 1 - \alpha \\ m_2 = \alpha. \end{cases} \quad (5)$$

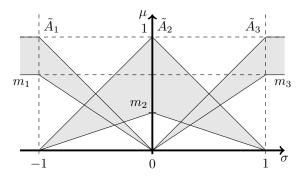Fig. 3. Structure of the SI-IT2-FPID position controller.

Fig. 4. Triangular IT2-FSs.

Thus, α is the only parameter to be adjusted in IT2-FLC.

The implemented SI-IT2-FLCs use the center of sets type reduction method [25], thus the output can be calculated as:

$$\varphi = \frac{\varphi^l + \varphi^r}{2}, \quad (6)$$

where φ^l and φ^r are the end points of the type reduced set which are defined as follows:

$$\begin{cases} \varphi^l &= \frac{\sum_{i=1}^{L} \overline{\mu}_{\tilde{A}_i}(\sigma) B_i + \sum_{i=L+1}^{N} \underline{\mu}_{\tilde{A}_i}(\sigma) B_i}{\sum_{i=1}^{L} \overline{\mu}_{\tilde{A}_i}(\sigma) + \sum_{i=L+1}^{N} \underline{\mu}_{\tilde{A}_i}(\sigma)} \\ \varphi^r &= \frac{\sum_{i=1}^{R} \underline{\mu}_{\tilde{A}_i}(\sigma) B_i + \sum_{i=R+1}^{N} \overline{\mu}_{\tilde{A}_i}(\sigma) B_i}{\sum_{i=1}^{R} \underline{\mu}_{\tilde{A}_i}(\sigma) + \sum_{i=R+1}^{N} \overline{\mu}_{\tilde{A}_i}(\sigma)}, \end{cases} \quad (7)$$

where L and R are the switching points [25]. As shown in Fig. 4, the SI-IT2-FLCs employs fully overlapping IT2-FSs in the sense of LMFs and UMFs. Therefore, it is guaranteed that a crisp value σ always belongs to two successive IT2-FSs ($\tilde{A}_i$ and $\tilde{A}_{i+1}$). Consequently, the values of L and R are equal to 1 since only $N = 2$ rules will be always activated [26].

The FM of the SI-IT2-FLC $\varphi(\sigma)$ has been derived in [19] as follows:

$$\varphi(\sigma) = \sigma k (|\sigma|), \quad (8)$$

where $k(\sigma)$ is the nonlinear gain defined as:

$$k(\sigma) = \frac{1}{2} \left(\frac{1}{\alpha + \sigma - \alpha\sigma} + \frac{\alpha - 1}{\alpha\sigma - 1} \right). \quad (9)$$

Remark 2. *The formulation above reduces the design of IT2-FLC into a control curve (CC) generation.*

Defining $\varepsilon(\sigma) = \varphi(\sigma) - \sigma$, the following analysis is done:
1) If $0 < \alpha \leq \alpha_{c1}$, then $\varepsilon > 0$ for $\forall \sigma \in [0, 1)$, where $\alpha_{c1} = \frac{3 - \sqrt{5}}{2} \approx 0.382$. Thus, an aggressive CC (A-CC) will be generated.
2) If $\alpha_{c2} \leq \alpha < 1$, then $\varepsilon < 0$ for $\forall \sigma \in [0, 1)$, where $\alpha_{c2} = \frac{\sqrt{5} - 1}{2} \approx 0.618$. Thus, a smooth CC (S-CC) will be generated.
3) If $\alpha_{c1} < \alpha < \alpha_{c2}$, then $\varepsilon > 0$ for $\forall \sigma \in [0, 0.5)$ and $\varepsilon < 0$ for $\forall \sigma \in [0.5, 1)$. Thus, a moderate CC (M-CC) will be generated.

In Fig. 5, A-CC, S-CC, and M-CC are illustrated. When σ is close to 0, A-CC has relatively high input sensitivity in comparison to S-CC. On the other hand, A-CC has a low sensitivity when the input signal is close to ± 1, while S-CC
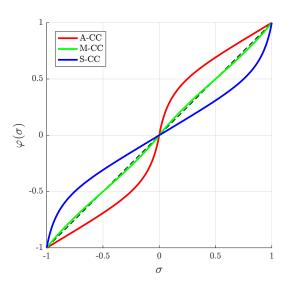
Fig. 5. Illustration of the control curves.

has a high sensitivity in the region close to ± 1. Finally, M-CC is a combination of S-CC and A-CC. Thus, it has a low sensitivity when the error signal is close to ± 1, while a high sensitivity when the error signal is close to '0'.

Definition 1. *Let $f(\mathbf{x})$ be a real-valued function of a real variable $\mathbf{x}$, then f is an odd symmetrical iff $f(-\mathbf{x}) = -f(\mathbf{x})$.*

Lemma 1. *Any linear combination of odd functions $g(\mathbf{x}) = \sum_i a_i f_i(\mathbf{x})$ is an odd function, where a_i are scalars.*

Proof. By Definition 1 $f_i(-\mathbf{x}) = -f_i(\mathbf{x})$; therefore, $g(-\mathbf{x}) = \sum_i a_i f_i(-\mathbf{x}) = -\sum_i a_i f_i(\mathbf{x}) = -g(\mathbf{x})$. $\square$

Theorem 1. *If $u(\sigma_p, \sigma_i, \sigma_d)$ in (3) denotes FM of SI-IT2-FPID, then $u(\sigma_p, \sigma_i, \sigma_d)$ is a symmetrical odd function w.r.t. its input variable σ_p, σ_i and σ_d, i.e., $u(-\sigma_p, -\sigma_i, -\sigma_d) = -u(\sigma_p, \sigma_i, \sigma_d) \quad \forall \sigma_p, \sigma_i, \sigma_d \in \mathbb{R}$.*

Proof. Let's prove that $\varphi(\sigma)$ in (8) is symmetrical odd function: $\varphi(-\sigma) = -\sigma k(|\sigma|) = -\varphi(\sigma)$. From (3) it's possible to observe that u is a linear combination of φ; therefore, by using Lemma 1, u is a symmetrical odd function. $\square$

Definition 2. *Let $f(\mathbf{x})$ be a real-valued function of a real variable $\mathbf{x}$, then f is continuous iff $\lim_{\mathbf{x} \to \mathbf{c}} f(\mathbf{x}) = l$.*

Lemma 2. *Any linear combination of continuous functions $g(\mathbf{x}) = \sum_i a_i f_i(\mathbf{x})$ is a continuous function.*

Proof. By Definition 2 $\lim_{\mathbf{x} \to \mathbf{c}} f_i(\mathbf{x}) = l_i$; therefore, $\lim_{\mathbf{x} \to \mathbf{c}} g(\mathbf{x}) = \lim_{\mathbf{x} \to \mathbf{c}} \sum_i a_i f_i(\mathbf{x}) = \sum_i a_i \lim_{\mathbf{x} \to \mathbf{c}} f_i(\mathbf{x}) = \sum_i a_i l_i$. $\square$

Theorem 2. *If $u(\sigma_p, \sigma_i, \sigma_d)$ in (3) denotes FM of SI-IT2-FPID, then $u(\sigma_p, \sigma_i, \sigma_d)$ is a continuous function in the region $[-1, 1]^3$ w.r.t. its input variables σ_p, σ_i and σ_d, i.e., $u \in \mathcal{C}^0([-1, 1]^3) \quad \forall \alpha_p, \alpha_i, \alpha_d \in (0, 1)$.*

Proof. First, let's prove that $\varphi(\sigma)$ in (8) is a continuous function $\forall \sigma \in [-1, 1]$ and $\forall \alpha \in (0, 1)$. It has two vertical asymptotes when $\alpha + |\sigma| - \alpha|\sigma| = 0$ or $\alpha\sigma - 1 = 0$, or rather $|\sigma| = -\frac{\alpha}{1-\alpha}$ or $|\sigma| = \frac{1}{\alpha}$. The first condition is never true because $-\frac{\alpha}{1-\alpha} < 0 \quad \forall \alpha \in (0, 1)$ and $|\sigma| \geq 0 \quad \forall \sigma$. The second condition is also never true because $\frac{1}{\alpha} > 1 \quad \forall \alpha \in (0, 1)$ and $|\sigma| \leq 1 \quad \forall \sigma \in [-1, 1]$. Therefore, $\varphi(\sigma)$ is a continuous function $\forall \sigma \in [-1, 1]$ and $\forall \alpha \in (0, 1)$. From (3) it's possible to observe that u is a linear combination of φ; therefore, by using Lemma 2, u is a continuous function. $\square$

Definition 3. *Let $f(\mathbf{x})$ be a real-valued function of a real variable $\mathbf{x}$, then f is strictly increasing iff $\frac{\partial f(\mathbf{x})}{\partial \mathbf{x}} > 0$.*

Lemma 3. *A sum of strictly increasing functions $g(\mathbf{x}) = \sum_i a_i f_i(\mathbf{x})$ is a strictly increasing function, $\forall a_i \geq 0$.*

Proof. By Definition 3 $\frac{\partial f_i(\mathbf{x})}{\partial \mathbf{x}} > 0$; therefore, $\frac{\partial g(\mathbf{x})}{\partial \mathbf{x}} = \frac{\partial \sum_i a_i f_i(\mathbf{x})}{\partial \mathbf{x}} = \sum_i a_i \frac{\partial f_i(\mathbf{x})}{\partial \mathbf{x}} > 0 \quad \forall a_i \geq 0$. $\square$

Theorem 3. *If $u(\sigma_p, \sigma_i, \sigma_d)$ in (3) denotes FM of SI-IT2-FPID, then $u(\sigma_p, \sigma_i, \sigma_d)$ is a strictly increasing function in the region $[-1, 1]^3$ w.r.t. its input variables σ_p, σ_i and σ_d, i.e., $\frac{\partial u}{\partial \sigma_p} > 0, \frac{\partial u}{\partial \sigma_i} > 0, \frac{\partial u}{\partial \sigma_d} > 0 \quad \forall \alpha_p, \alpha_i, \alpha_d \in (0, 1)$.*

Proof. First, let's prove that $\varphi(\sigma)$ in (8) is a strictly increasing function $\forall \sigma \in [-1, 1]$ and $\forall \alpha \in (0, 1)$: $\frac{\partial \varphi}{\partial \sigma} = \frac{1}{2} \left(\frac{1}{\alpha + |\sigma| - \alpha|\sigma|} + \frac{\alpha - 1}{\alpha|\sigma| - 1} - \frac{|\sigma| - \alpha|\sigma|}{(\alpha + |\sigma| - \alpha|\sigma|)^2} - \frac{\alpha|\sigma|(\alpha - 1)}{(\alpha|\sigma| - 1)^2} \right)$ (by observing that $\text{sign}(\sigma)\sigma = |\sigma|$). After further simplifications, $\frac{\partial \varphi}{\partial \sigma} = \frac{1}{2} \left(\frac{1-\alpha}{(\alpha + |\sigma| - \alpha|\sigma|)^2} + \frac{\alpha}{(\alpha|\sigma| - 1)^2} \right)$ in which $\frac{1-\alpha}{(\alpha + |\sigma| - \alpha|\sigma|)^2} \geq 0$ and $\frac{\alpha}{(\alpha|\sigma| - 1)^2} \geq 0 \quad \forall \alpha \in (0, 1)$. Therefore, by using Lemma 3, $\varphi(\sigma)$ is a strictly increasing function. From (3) it's possible to observe that u is a sum of $k\varphi$, where $k > 0$; therefore, by using again Lemma 3, u is a strictly increasing function. $\square$

Corollary 1. *If $u(\sigma_p, \sigma_i, \sigma_d)$ in (3) denotes FM of SI-IT2-FPID, then $\frac{\partial u}{\partial \sigma_p}$, $\frac{\partial u}{\partial \sigma_i}$ and $\frac{\partial u}{\partial \sigma_d}$ are continuous functions in the region $[-1, 1]$ w.r.t. its input variables σ_p, σ_i and σ_d, i.e., $u \in \mathcal{C}^1([-1, 1]^3) \quad \forall \alpha_p, \alpha_i, \alpha_d \in (0, 1)$.*

We have also analysed the resulting CSs as the control signal is a linear combination of the outputs from SI-IT2-FLCs as given in (3). In order to clearly show the effect of the FOU parameters, we have set and fixed $k_p = k_d = 1$ and $k_i = 0$ and investigated the resulting CSs. Fig. 6 shows the CSs which maps the two inputs σ_p and σ_d to the output u. To generate the CSs, aggressive, moderate and smooth values of α_p and α_d are chosen for φ_p and φ_d, it can be observed that it is possible easily generate various types of CSs by simply changing the FOU parameter of each SI-IT2-FLC.

For the presented CSs in Fig. 6, it can be observed that:

1) PS-1 ($\alpha_p = 0.25$, $\alpha_d = 0.25$): both φ_p and φ_d are defined with A-CCs. Therefore, the resulting controller will have a fast response time. However, the control system might not be robust against noise and uncertainties.

2) PS-2 ($\alpha_p = 0.25$, $\alpha_d = 0.5$): φ_p and φ_d are defined with an A-CC and M-CC, respectively. Therefore, the
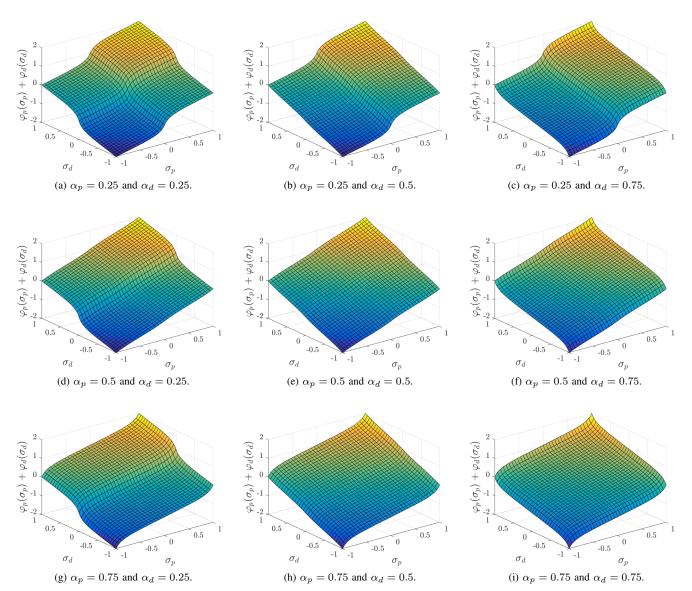
Fig. 6. Illustration of the CSs with aggressive, moderate and smooth values of α_p and α_d for φ_p and φ_d, respectively.

proportional action will be more aggressive than its derivative counterpart and the resulting controller will be more sensitive to the noise in comparison with PS-1.

3) PS-3 ($\alpha_p = 0.25$, $\alpha_d = 0.75$): φ_p and φ_d are defined with an A-CC and S-CC, respectively. Therefore, the proportional action will be always more aggressive than its derivative counterpart and the resulting system response of the controller will be fast but at the same time may lead to the instability of the system. This PS is the most aggressive one.

4) PS-4 ($\alpha_p = 0.5$, $\alpha_d = 0.25$): φ_p and φ_d are defined with an M-CC and an A-CC, respectively. Therefore, the input sensitivity of the derivative action will be relatively higher as the system approaches the reference value and the resulting response of the controller will be robust.

5) PS-5 ($\alpha_p = 0.5$, $\alpha_d = 0.5$): both φ_p and φ_d are defined with M-CCs. Therefore, the resulting controller will increase the damping when the error is small, which will enhance the system response, but will decrease the damping when the error is large.

6) PS-6 ($\alpha_p = 0.5$, $\alpha_d = 0.75$): φ_p and φ_d are defined with an M-CC and S-CC, respectively. Therefore, the proportional part will be stronger than its derivative counterpart and the resulting controller will be more sensitive to the noise but faster in comparison with PS-5.

7) PS-7 ($\alpha_p = 0.75$, $\alpha_d = 0.25$): φ_p and φ_d are defined with an S-CC and A-CC, respectively. Therefore, the derivative action will be always more aggressive than its proportional counterpart and the resulting system response of the controller will result without overshoot but with a relatively bigger rise time value. This PS is the smoothest one.

8) PS-8 ($\alpha_p = 0.75$, $\alpha_d = 0.5$): φ_p and φ_d are defined with an S-CC and an M-CC, respectively. Therefore, the sensitivity of the derivative action will be relatively higher as the system approaches the reference value and the

resulting system response of the controller will be faster in comparison with PS-7.

9) PS-9 ($\alpha_p = 0.75$, $\alpha_d = 0.75$): both φ_p and φ_d are defined with S-CCs. Therefore, the resulting controller will be potentially more robust against parameter variations and disturbances in comparison with PS-8.

Remark 3. *It has to be noted that the parameters α_p and α_d are not functional in the same way with k_p and k_d coefficients of a PD controller. If we decrease the value of α_p or α_d, the correspondent part will have more aggressive action. On the other side, if we increase the value of α_p or α_d, the behaviour of the correspondent part will be smoother.*

In the light of the presented derivations and analyses, it can be concluded that the SI-IT2-FPID keeps the most preferred features of the PID such as simplicity and easy implementation. Moreover, it has been mathematically shown there exist an interpretable relationship between antecedent IT2-FSs and the controller output which clearly shows the design simplicity of the controller. The SI-IT2-FPID also preserves the ability of independent gain tuning of the conventional PID controller. Thus, by simply adjusting the extra degrees of freedom provided by the IT2-FSs, the control actions of the SI-IT2-FPID can be simply designed independently in straight forward manner. We believe these features are crucial especially in the fine-tuning phase in real-time applications.

Remark 4. *The analysis made in the paper has motivated us to use the control scheme in Fig. 3.*

IV. EXPERIMENTAL RESULTS

A. Trajectory Generation

In the experimental scenario, a square-shaped 3D trajectory with the length of the square's side of 2m is chosen to test the stability and robustness of each controller. The navigation of the UAV combines several manoeuvres such as hovering, straight line path as well as climbing and descending movements. The trajectory is made of eight way-points, located at $[1,1,0.8]$m, $[1,0,0.8]$m, $[1,-1,0.8]$m, $[0,-1,1]$m, $[-1,-1,1.2]$m, $[-1,0,1.2]$m, $[-1,1,1.2]$m and $[0,1,1]$m. First, the UAV hovers at $[1,1,0.8]$m. After that, the UAV flies to the next way-point at $[1,0,0.8]$m and hovers for 10s before flying to the next way-point.

B. Experimental Setup

The laboratory environment, shown in Fig. 7, is designed to use the motion capture system to provide the real-time pose of the UAV. The system is comprised of an array of eight OptiTrack Prime 13 cameras. The cameras monitor the quadcopter's six degrees of freedom: x, y and z coordinates and roll ϕ, pitch θ and yaw ψ orientation. The cameras provide a new reading at 120Hz. Then, the ground station computes the control signal and provides it to the UAV at 100Hz rate. The aerial vehicle used for the experimental flight tests is the Parrot Bebop 2 aircraft, shown in Fig. 7, which is a UAV controlled via a Wi-Fi connection. The command input is routed to the Bebop 2 and wireless network. The ROS environment is used to communicate with the Bebop.
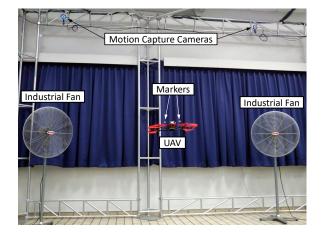

Fig. 7. Experimental setup.

The control gains in (3) for each control axis (x, y and z) are tuned and set to: $k_p = 2.0$, $k_i = 0.1$ and $k_d = 0.6$. In addition, the maximum position error in our application is 2m, therefore, the input scaling factor is set to: $k_e = \frac{1}{2}$.

The control performance evaluation is carried out in terms of the root mean squared error (RMSE) of the 3D position:

$$e_{\text{RMSE}} = \sqrt{\frac{\sum_{i=1}^{N} \|\mathbf{e}_i\|^2}{N}}, \qquad (10)$$

where N is the number of samples, $\mathbf{e}_i = \mathbf{p}_i^* - \mathbf{p}_i$, $\mathbf{p}_i^*$ and $\mathbf{p}_i$ are the desired and actual position for the i-th sample, respectively. In addition, the controllers are compared in terms of the total variation of the control signal:

$$V = \sum_{i=1}^{N-1} \left(|\phi_{i+1}^* - \phi_i^*| + |\theta_{i+1}^* - \theta_i^*| + |v_{z,i+1}^* - v_{z,i}^*| \right), \qquad (11)$$

where ϕ_i^*, θ_i^* and $v_{z,i}^*$ are pitch, roll and vertical velocity for the i-th sample, respectively.

C. Trajectory Tracking in Absence of Wind

In order to validate the theoretical analysis, we present experimental validations for the described nine FOU PSs given in Section III. In the experimental results, we have fixed the FOU parameter of the integral action $\alpha_i = 0.5$, since the control gain of the integral part k_i is very small.

The position (x, y and z) responses of the designed SI-IT2-FPID controllers with PS-1, PS-3, PS-5, PS-7, and PS-9 are shown in Fig. 8. As it can be observed from Fig. 8, the controllers with aggressive φ_p (PS-1 and PS-3) have an oscillatory behavior, while the controllers with smooth φ_p (PS-7 and PS-9) are relatively slow in converging to the final value as expected. On the other hand, the controller with moderate φ_p (PS-5) combines the characteristics of both aggressive and smooth controllers, it is fast with small oscillations and overshoots. Therefore, it can be concluded that the experimental results prove the theoretical expectations. The average RMSE of ten experiments for each case are given in Table I. As can be seen from this table, SIT2-FPID with PS-5 resulted in the lowest RMSE value. The total variations of control signal of
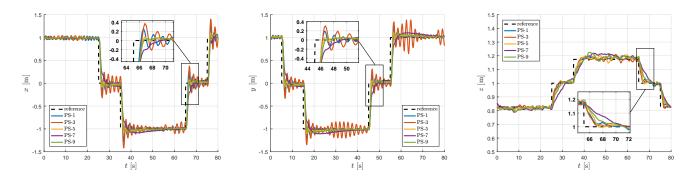
Fig. 8. Trajectory tracking for x, y and z axes of SI-IT2-FPID position controllers with different values of α_p and α_d in absence of wind.

ten experiments for each case are given in Table II. As can be seen from this table, the controllers with more aggressive CS resulted in the higher signal variation, while the controllers with smoother CS resulted in the lower signal variation.

In order to show the efficacy and efficiency of the SI-IT2-FPID controllers, they are compared with the standard PID controller and T1-FPID. The control gains for all controllers are tuned properly for the square-shaped trajectory. The trajectory tracking result is shown in Fig. 9. The average RMSE of ten experiments for each case are given in Table I.

Remark 5. *As it has been underlined throughout the paper, the main goal of this research is to show that the SI-IT2-FPID structure is easy to design and feasible to deploy especially in real-time control systems and not to show that control performance of the SI-IT2-FPID superior in comparison to its type-1 and conventional counterparts. We have provided only the experimental results of the PID and T1-FPID structures for the completeness of the paper.*

D. Trajectory Tracking in Presence of Wind

The responses to different SI-IT2-FPID controllers in the presence of unmodeled disturbances (induced wind disturbances, the maximum wind speed is $4.5\,\text{m/s}$) are given in Fig. 10. Therefore, it can be concluded that the experimental
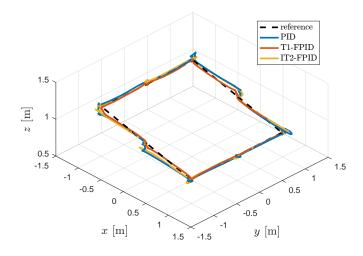

Fig. 9. Trajectory tracking in 3D space in absence of wind.

results prove the theoretical expectations. The average RMSE of ten experiments for each case are given in Table III. As can be seen from this table, SI-IT2-FPID with PS-4 is as good as SI-IT2-FPID with PS-5. The total variations of control signal of ten experiments for each case are given in Table IV. As can be seen from this table, the controllers with more aggressive CS resulted in the higher signal variation, while the controllers

TABLE I
AVERAGE RMSE IN ABSENCE OF WIND (UNIT: m).

	SI-IT2-FPID			PID	T1-FPID
α_p	α_d				
	0.25	**0.5**	**0.75**		
0.25	0.363	0.410	0.436		
0.5	0.355	**0.348**	0.352	0.359	0.358
0.75	0.401	0.390	0.372		

TABLE III
AVERAGE RMSE IN PRESENCE OF WIND (UNIT: m).

	SI-IT2-FPID			PID	T1-FPID
α_p	α_d				
	0.25	**0.5**	**0.75**		
0.25	0.490	0.484	0.603		
0.5	**0.367**	**0.367**	0.409	0.387	0.386
0.75	0.424	0.392	0.385		

TABLE II
TOTAL VARIATION OF CONTROL SIGNAL IN ABSENCE OF WIND.

	SI-IT2-FPID			PID	T1-FPID
α_p	α_d				
	0.25	**0.5**	**0.75**		
0.25	396.28	374.29	368.89		
0.5	163.23	97.62	89.91	76.58	43.07
0.75	63.05	55.30	50.20		

TABLE IV
TOTAL VARIATION OF CONTROL SIGNAL IN PRESENCE OF WIND.

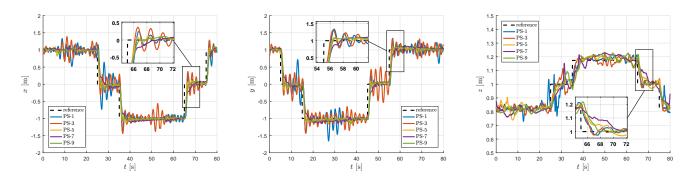|	SI-IT2-FPID			PID	T1-FPID
α_p	α_d				
	0.25	**0.5**	**0.75**		
0.25	432.40	425.86	419.23		
0.5	231.12	129.79	112.89	109.94	94.07
0.75	98.07	93.29	70.69		

Fig. 10. Trajectory tracking for x, y and z axes of SI-IT2-FPID position controllers with different values of α_p and α_d in presence of wind. The experimental video is available at https://youtu.be/Hz3f8N-30dg.

with smoother CS resulted in the lower signal variation.

In order to check the potential of SI-IT2-FPID controllers in the presence of unmodeled disturbances (induced wind disturbances), the trajectory tracking is shown in Fig. 11. The average RMSE of ten experiments for each case are given in Table III.

V. CONCLUSION

In this paper, we have extended the analysis for SI-IT2-FPID controllers by providing the effect of the FOU parameters on CS generation. In addition, we have shown that by only changing a single parameter which shapes the FOU, it is possible to generate different CSs. In order to validate our theoretical analysis and to show the design simplicity, we have conducted extensive comparative real world flight tests. Therefore, the SI-IT2-FPID controller has been designed and implemented in ROS environment using C++ for the position control of a quadcopter UAV. The real-time experimental results clearly show that the theoretical analysis of SI-IT2-FPID controllers coincides with the real-time experimental results. Moreover, the SI-IT2-FPID can achieve better control performance in presence of uncertainties and strong wind
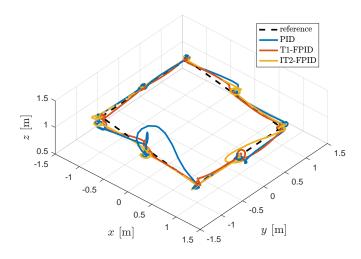
conditions when compared to its type-1 and conventional counterparts. We believe that the results of this paper are not only important for the type-2 fuzzy logic community but also for the control engineering community as it provides a simple but effective way to tune IT2-FLCs to obtain a satisfactory performance and also shows that the IT2-FLC structure can be implemented in real-time. Finally, all developed code is available on-line at https://github.com/andriyukr/FLC.

As a future work, we plan to work on optimization-based design methods in which it will be aimed to maximize both the control system performance and interpretability of IT2-FLCs.

Fig. 11. Trajectory tracking in 3D space in presence of wind.

REFERENCES

[1] L. Wang and Z. Zhang, "Automatic detection of wind turbine blade surface cracks based on uav-taken images," *IEEE Transactions on Industrial Electronics*, vol. PP, no. 99, pp. 1–1, 2017.
[2] S. Chen, F. Wu, L. Shen, J. Chen, and S. D. Ramchurn, "Decentralized patrolling under constraints in dynamic environments," *IEEE Transactions on Cybernetics*, vol. 46, no. 12, pp. 3364–3376, Dec 2016.
[3] S. Zhao, Z. Hu, M. Yin, K. Z. Y. Ang, P. Liu, F. Wang, X. Dong, F. Lin, B. M. Chen, and T. H. Lee, "A robust real-time vision system for autonomous cargo transfer by an unmanned helicopter," *IEEE Transactions on Industrial Electronics*, vol. 62, no. 2, pp. 1210–1219, Feb 2015.
[4] Y. Song, X. Huang, and C. Wen, "Robust Adaptive Fault-Tolerant PID Control of MIMO Nonlinear Systems With Unknown Control Direction," *IEEE Transactions on Industrial Electronics*, vol. 64, no. 6, pp. 4876–4884, June 2017.
[5] M. A. M. Cheema, J. E. Fletcher, D. Xiao, and M. F. Rahman, "A Linear Quadratic Regulator-Based Optimal Direct Thrust Force Control of Linear Permanent-Magnet Synchronous Motor," *IEEE Transactions on Industrial Electronics*, vol. 63, no. 5, pp. 2722–2733, May 2016.
[6] M. Mehndiratta and E. Kayacan, "Receding horizon control of a 3 DOF helicopter using online estimation of aerodynamic parameters," *Proceedings of the Institution of Mechanical Engineers, Part G: Journal of Aerospace Engineering*, 2017.
[7] E. Kayacan and R. Maslim, "Type-2 fuzzy logic trajectory tracking control of quadrotor vtol aircraft with elliptic membership functions," *IEEE/ASME Transactions on Mechatronics*, vol. 22, no. 1, pp. 339–348, Feb 2017.
[8] L. Cervantes and O. Castillo, "Type-2 fuzzy logic aggregation of multiple fuzzy controllers for airplane flight control," *Information Sciences*, vol. 324, pp. 247 – 256, 2015.

[9] V. N. N, A. Panda, and S. P. Singh, "A Three-Level Fuzzy-2 DTC of Induction Motor Drive Using SVPWM," *IEEE Transactions on Industrial Electronics*, vol. 63, no. 3, pp. 1467–1479, March 2016.

[10] C. H. Huang, W. J. Wang, and C. H. Chiu, "Design and Implementation of Fuzzy Control on a Two-Wheel Inverted Pendulum," *IEEE Transactions on Industrial Electronics*, vol. 58, no. 7, pp. 2988–3001, July 2011.

[11] A. Sarabakha, C. Fu, and E. Kayacan, "Double-Input Interval Type-2 Fuzzy Logic Controllers: Analysis and Design," in *2017 IEEE International Conference on Fuzzy Systems (FUZZ-IEEE)*, July 2017, pp. 1–6.

[12] S. Bhattacharyya, D. Basu, A. Konar, and D. Tibarewala, "Interval type-2 fuzzy logic based multiclass ANFIS algorithm for real-time EEG based movement control of a robot arm," *Robotics and Autonomous Systems*, vol. 68, pp. 104–115, 2015.

[13] O. Castillo, L. Amador-Angulo, J. R. Castro, and M. Garcia-Valdez, "A comparative study of type-1 fuzzy logic systems, interval type-2 fuzzy logic systems and generalized type-2 fuzzy logic systems in control problems," *Information Sciences*, vol. 354, pp. 257–274, 2016.

[14] O. Castillo and P. Melin, "A review on interval type-2 fuzzy logic applications in intelligent control," *Information Sciences*, vol. 279, pp. 615–631, 2014.

[15] A. Sarabakha, N. Imanberdiyev, E. Kayacan, M. A. Khanesar, and H. Hagras, "Novel Levenberg-Marquardt Based Learning Algorithm for Unmanned Aerial Vehicles," *Information Sciences*, vol. 417, pp. 361 – 380, 2017.

[16] C. Fu, A. Sarabakha, E. Kayacan, C. Wagner, R. John, and J. M. Garibaldi, "Similarity-Based Non-Singleton Fuzzy Logic Control for Improved Performance in UAVs," in *2017 IEEE International Conference on Fuzzy Systems (FUZZ-IEEE)*, July 2017, pp. 1–6.

[17] Y. Yang and Y. Yan, "Attitude regulation for unmanned quadrotors using adaptive fuzzy gain-scheduling sliding mode control," *Aerospace Science and Technology*, vol. 54, pp. 208 – 217, 2016.

[18] Y. Yang, J. Wu, and W. Zheng, "Trajectory tracking for an autonomous airship using fuzzy adaptive sliding mode control," *Journal of Zhejiang University SCIENCE C*, vol. 13, no. 7, pp. 534–543, Jul 2012.

[19] T. Kumbasar, "Robust Stability Analysis and Systematic Design of Single-Input Interval Type-2 Fuzzy Logic Controllers," *IEEE Transactions on Fuzzy Systems*, vol. 24, no. 3, pp. 675–694, June 2016.

[20] T. N. Dief, M. G. Abdelhady, and S. Yoshida, "Attitude and altitude stabilization of quad rotor using parameter estimation and self-tuning controller," in *AIAA Atmospheric Flight Mechanics Conference*, 2015, p. 2392.

[21] R. Mahony, V. Kumar, and P. Corke, "Multirotor Aerial Vehicles: Modeling, Estimation, and Control of Quadrotor," *Robotics Automation Magazine, IEEE*, vol. 19, no. 3, pp. 20–32, 2012.

[22] S. Bouabdallah, "Design and control of quadrotors with application to autonomous flying," Ph.D. dissertation, EPFL, Dec 2007.

[23] A. Sarabakha and E. Kayacan, "Y6 Tricopter Autonomous Evacuation in an Indoor Environment Using Q-Learning Algorithm," in *Decision and Control (CDC), 55th IEEE Conference on*, Dec 2016.

[24] T. Kumbasar and H. Hagras, "Big Bang-Big Crunch optimization based interval type-2 fuzzy PID cascade controller design strategy," *Information Sciences*, vol. 282, pp. 277 – 295, 2014.

[25] J. Mendel, *Uncertain rule-based fuzzy logic system: introduction and new directions*. Upper Saddle River, NJ, USA, Prentice-Hall, 2001.

[26] T. Kumbasar, "A Simple Design Method for Interval Type-2 Fuzzy PID Controllers," *Soft Computing*, vol. 18, no. 7, pp. 1293–1304, 2014.

Changhong Fu (M'16) was born in Hunan, China, on July 31, 1986. He received his Ph.D. degree in Robotics and Automation from Technical University of Madrid, Madrid, Spain, in 2015. He is currently a Post-doctoral Research Fellow with school of Mechanical and Aerospace Engineering and ST Engineering - NTU Corp Lab in Nanyang Technological University (NTU), Singapore.

He has worked on 8 different types of projects related to the vision for UAVs. His research interests include visual tracking, odometry, SLAM and intelligent control for UAV autonomy.

Erdal Kayacan (S'06–SM'12) holds a PhD in Electrical and Electronic Engineering from Bogazici University (2011). He was a visiting scholar in University of Oslo in 2009 with the research fellowship of Norway Research Council. After his post-doctoral research in KU Leuven at the Division of Mechatronics, Biostatistics and Sensors, Dr. Kayacan went on to pursue his research in Nanyang Technological University at the School of Mechanical and Aerospace Engineering as assistant professor (2014 - current).

He has published more than 90 peer-refereed book chapters, journal and conference papers in intelligent control, fuzzy systems and robotics. In the area of artificial intelligence in system identification and control theory as applied to robotic applications, his contributions to interval type-2 fuzzy neural networks have made a notable impact on the computational intelligence community and have also reached a high level of international recognition. Dr. Kayacan is co-writer of a course book "Fuzzy Neural Networks for Real Time Control Applications, 1st Edition Concepts, Modeling and Algorithms for Fast Learning", Butterworth-Heinemann, Print Book. He is a Senior Member of Institute of Electrical and Electronics Engineers (IEEE). From 1st Jan 2017, he is an Associate Editor of IEEE Transactions on Fuzzy Systems, the leading international journal in artificial intelligence.

Tufan Kumbasar (M'13) received the B.Sc. and M.Sc. and Ph.D. degrees in Control and Automation Engineering from the Istanbul Technical University. He is currently an Assistant Professor in the Control and Automation Engineering Department, Faculty of Electrical and Electronics Engineering, Istanbul Technical University.

His major research interests are in computational intelligence, notably type-2 fuzzy systems, fuzzy control, neural networks, evolutionary algorithms and control theory. He is also interested in process control, robotics, intelligent control and their real-world applications. He has currently authored more than 70 papers in international journals, conferences and books. Dr. Kumbasar received the Best Paper Award from the IEEE International Conference on Fuzzy Systems in 2015.

Andriy Sarabakha (S'16) was born in Lviv, Ukraine, on November 16, 1986. He received a B.Sc. degree in Computer Engineering in 2012 from "Sapienza" - University of Rome, Rome, Italy, as well as a M.Sc. degree in Artificial Intelligence and Robotics in 2015 from the same university. From January 2016, he is pursuing his research in Nanyang Technological University, Singapore, at the School of Mechanical and Aerospace Engineering as Ph.D. student.

His research areas are unmanned aerial vehicles, artificial intelligence and fuzzy logic.